engineering proceedings

MDPI

Proceeding Paper

First-Principle Calculation Analysis on Electronic Structures and Molecular Dynamics of Gadolinium-Doped $FAPbI_3$ †

Atsushi Suzuki * and Takeo Oku

Department of Materials Chemistry, The University of Shiga Prefecture, 2500 Hassaka, Hikone 522-8533, Shiga, Japan; oku@mat.usp.ac.jp

* Correspondence: suzuki@mat.usp.ac.jp; Tel.: +81-749-28-8369

† Presented at the 4th International Electronic Conference on Applied Sciences, 27 October–10 November 2023; Available online: https://asec2023.sciforum.net/.

Abstract: First-principle calculation analysis on electronic structures and molecular dynamics was performed to investigate the addition of gadolinium ion into a formamidinium lead iodine ($FAPbI_3$) perovskite crystal for use in the application of photovoltaic devices with stability of performance. Band dispersion, density of state, enthalpy, and kinetic energy were predicted during the relaxation process. The Gd^{2+}-doped $FAPbI_3$ perovskite crystal had an effective mass ratio of 0.02 in narrow band dispersion, consisting of 5d and 4f orbitals of gadolinium ion, a 6p orbital of lead ion, and a 5p orbital of iodine ion, supporting the charge transfer and carrier diffusion related to carrier mobility as a photovoltaic parameter. The molecular dynamics of the Gd^{2+}-doped perovskite crystal indicate dynamic stability while suppressing decomposition, with separation between nitrogen and hydrogen ions on FA in the crystal. The first-principle calculation predicts that it is advantageous to apply the Gd^{2+}-doped $FAPbI_3$ perovskite crystal to the perovskite solar cell, providing stability of photovoltaic performance.

Keywords: electronic structure; molecular dynamics; gadolinium; perovskite; photovoltaic property

Citation: Suzuki, A.; Oku, T. First-Principle Calculation Analysis on Electronic Structures and Molecular Dynamics of Gadolinium-Doped $FAPbI_3$. *Eng. Proc.* **2023**, *56*, 33. https://doi.org/10.3390/ASEC2023-15332

Academic Editor: Elisabeta Szerb

Published: 26 October 2023

1. Introduction

Metal halide perovskite crystal has been fabricated and characterized for the development of industrial materials using photovoltaic devices. Material design and performance prediction of perovskite crystal have been performed for the development of perovskite solar cells, optimizing the photovoltaic performance [1–10]. An electronic structure and band distribution with an effective mass ratio and band gap were expected, according to the first-principle calculation [11–14]. The photovoltaic properties were based on crystal structure, morphology, and 2/3-dimension interfacial formation [15]. The interface passivation on the crystal grain in the perovskite layer suppressed the carrier trap near defect and pinhole in the perovskite layer, extending carrier life and diffusion related to mobility as the photovoltaic parameters [16–23].

Lanthanide-doped perovskite crystals have been used for the development of electronic devices such as wavelength convertors, using ultra-visible-near-infrared absorption and luminescence [24–29]. The lanthanide ion in a multivalent state caused a shuttle redox reaction involving the redox of lead and halogen ion to regenerate crystal degradation. For example, a slight addition of europium, gadolinium (Gd^{2+}), samarium, and cerium ions suppressed decomposition with the shuttle redox reaction, reforming the perovskite crystal to achieve long-term stability of the performance [30,31]. The photovoltaic properties were also related to the band structure with an effective mass of the hole and electron. Molecular dynamics have been applied for predicting the reaction mechanism, crystal nucleation, formation, decomposition, and energies together with ion diffusion [32–39]. The purpose of this study is to focus on the characterization of band structure and molecular dynamics

of formamidinium lead iodide ($CH(NH_2)_2PbI_3$: $FAPbI_3$) perovskite crystal doped with Gd^{2+} ion for improving photovoltaic performance and stability.

2. Calculation

The Gd^{2+}-doped $FAPbI_3$ perovskite crystal was assembled with supercells ($2 \times 2 \times 2$) based on $FAPbI_3$ crystals as a cubic crystal phase (cubic $Pm\bar{3}m$) with experimental lattice constants ($FAPbI_3$: a = 6.3621 Å) [31,32,40–42]. Partial substitution of Gd^{2+} ions for a Pb^{2+} cation ion was introduced at the center of the cubic structure. The ab initio quantum calculations were performed using Vanderbilt ultrasoft pseudo-potentials, scalar relativistic generalized gradient approximations, and density functional theory (DFT) (Quantum Espresso, v.5.2.1, Quantum Espresso Foundation, UK). The band structures, effective mass ratio of electrons to free electrons, and holes to free electrons (m_e^*/m_e and m_h^*/m_e), band gap (E_g) and density of state (DOS) near valence (VB), and conduction band (CB) states were calculated.

Car-Parrinello molecular dynamics (CPMDs) simulations were performed using Quantum Espresso. Plane-wave basis set cutoffs for the smooth part of the wave functions and the augmented density were 80 and 320 Ry, respectively. The CPMD simulations were performed during an integration time step of 150 for a total simulation time of 0.018 psec. The enthalpy, kinetic energy, and molecular dynamics were followed during the relaxation process near 300 K.

3. Results and Discussion

The first-principle calculation analysis was performed to investigate the impact of the addition of a Gd^{2+} ion into perovskite crystal on the electron density distribution, band dispersion, and DOS. The electron density distribution of the Gd^{2+}-doped $FAPbI_3$ perovskite crystal is shown in Figure 1a. The partially occupied 6s, 6p, and 5d orbitals and fully occupied 4f orbital of a Gd^{2+} ion, and the partially occupied 5s and 5p orbitals of an iodine ion as a ligand, were distributed and overlapped each other, sharing the electron between the Gd^{2+} ion and iodine ion to form the coordination bond. Ligand–metal charge transfer between the Gd^{2+} ion and iodine ion was caused, supporting the carrier generation and diffusion related to carrier mobility as a photovoltaic parameter. The band dispersion and DOS are shown in Figure 1b,c. The 5p orbitals of the iodine ion were widely distributed in a range from −3 eV to −2 eV near the VB state, and the 6p orbital of lead ion and 5d orbitals and 4f orbital of the Gd^{2+} ion were also distributed in a range from 0 eV to 1.5 eV near the CB state. An effective mass ratio (m_e^*/m_e and m_h^*/m_e) was calculated to be 0.02 and 0.02 from the band dispersion near the VB and CB states. The direct band gap (E_g) at the Γ position as a *k*-vector was obtained to be about 1.52 eV, showing semi-conductive characteristics. The Gd^{2+}-doped $FAPbI_3$ crystal had narrow band dispersion with the same order of effective mass ratio, similar to those of the $FAPbI_3$ crystal. The photovoltaic performance related to the short circuit current density based on the carrier mobility was maintained. The formation energies of the Gd^{2+}-doped crystal and $FAPbI_3$ crystal were obtained to be -4662 eV cell^{-1} and -3745 eV cell^{-1}, which indicates the stability of the Gd^{2+}-doped $FAPbI_3$ crystal.

The enthalpy and kinetic energy of the Gd^{2+}-doped $FAPbI_3$ crystal and the $FAPbI_3$ crystal were calculated for predicting the crystal formation, dynamic stability, and kinetics of the reaction mechanism, such as decomposition. The dynamic behaviors regarding the enthalpy and kinetic energy during the relaxation time are shown in Figure 2a. In both cases, similar behavior of the kinetic energies was qualitatively demonstrated. The addition of a Gd^{2+} ion into the perovskite crystal caused a gradual decreasing behavior of the enthalpy during the relaxation time. The energy fluctuations were based on the crystal stability with slight distortion of the coordination structure. The kinetic energy behavior of the Gd^{2+}-doped $FAPbI_3$ crystal was similar to that of the $FAPbl_3$ crystal, indicating that the dynamic stability reached equilibrium in the final stage. The kinetic energy behavior was derived from the dynamic stability related to the degree of distortion of the coordination

structure with variation in the position of FA, the Gd^{2+} ion, and the iodine ion as the ligand. The structural distortions and molecular dynamics would have been suppressed by the addition of a Gd^{2+} ion. To make the dynamic behavior clear, the structural distortion of FA in the Gd^{2+}-doped $FAPbI_3$ crystal and $FAPbI_3$ crystal was characterized by a molecular dynamics calculation.

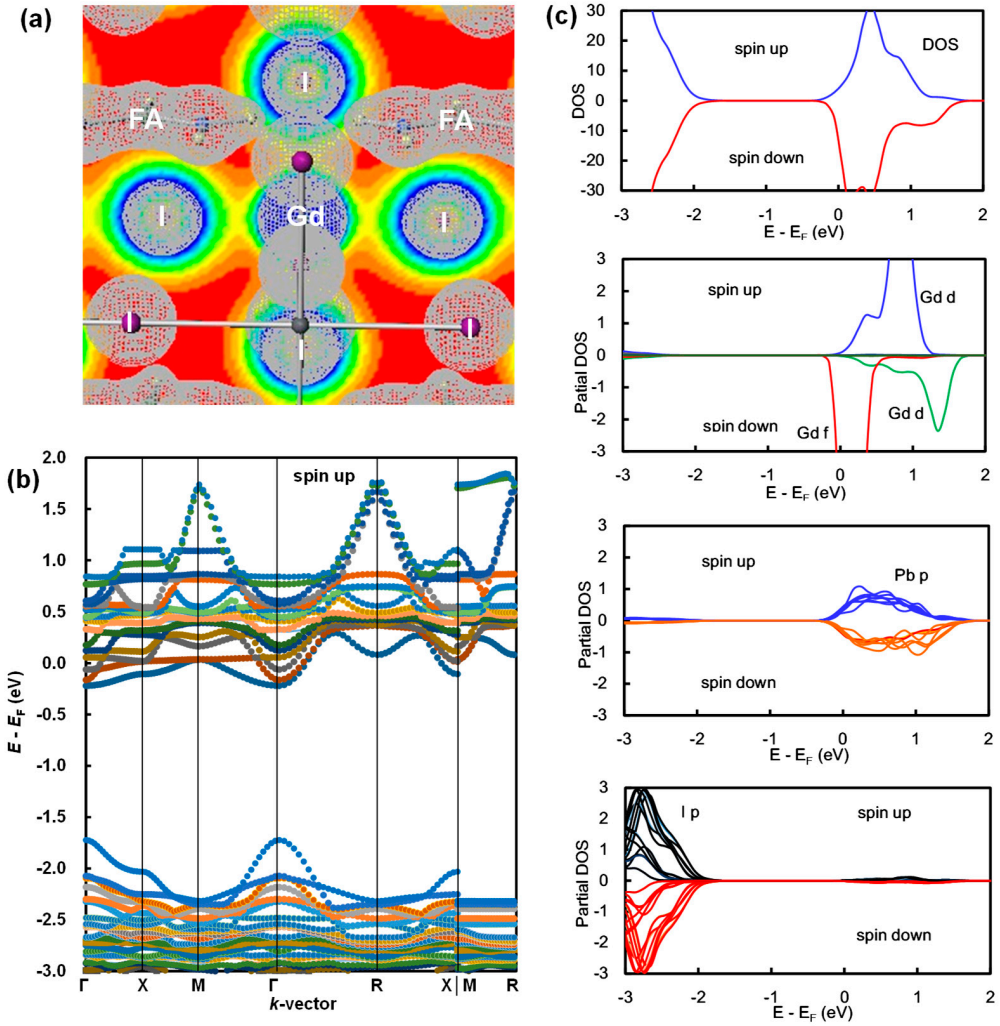

Figure 1. (**a**) Electron density distribution; (**b**) band dispersion; and (**c**) DOS of spin up (black and blue lines) and spin down (red and green lines) for the Gd^{2+}-doped $FAPbI_3$ perovskite crystal.

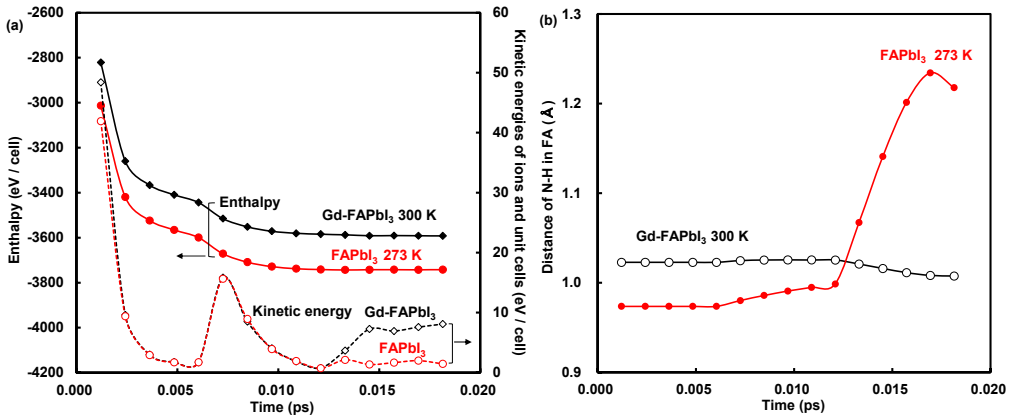

Figure 2. (**a**) Enthalpy, kinetic energy, and (**b**) distance of N-H in FA of (**b**) Gd^{2+}-doped $FAPbI_3$ crystal.

The distance of the nitrogen (N) and hydrogen (H) atom in the FA of the Gd^{2+}-doped $FAPbI_3$ crystal and $FAPbI_3$ crystal was considered, as shown in Figure 2b. In the case of the $FAPbI_3$ crystal, the distance of the N-H band in FA was drastically increased, meaning the separation between the N-H bands in FA at the time of 0.0169 psec. The atomic position of the Pb^{2+} ion located in the center of the $FAPbI_3$ crystal was shifted, shrinking the coordination structure in the perovskite crystal as the decomposition occurred. The distortion of crystal structures was induced with a reduction in the thermal energy. In the case of the Gd^{2+}-doped $FAPbI_3$ crystal, the distance between the N and H atom in FA was slightly decreased, showing the dynamic stability of FA. The atomic position of the Pb^{2+} ion located in the center of the coordination structure was maintained in the final stage. The addition of a Gd^{2+} ion into the crystal maintained stabilization, while suppressing the crystal distortions and the separation between N-H bands in FA as part of the decomposition. The calculation prediction indicates that it is advantageous to apply the Gd^{2+}-doped $FAPbI_3$ perovskite crystal to photovoltaic devices, providing stability of performance.

4. Conclusions

The first-principle calculation predicted the band dispersion, DOS, electron density distribution, enthalpy, kinetic energy, and molecular dynamics of the Gd^{2+}-doped $FAPbI_3$ crystal, as compared with those of the $FAPbI_3$ crystal. The Gd^{2+}-doped $FAPbI_3$ crystal had an effective mass ratio of 0.02 in the narrow band dispersion, consisting of a 5d orbital of the Gd^{2+} ion, 6p orbital of the Pb^{2+} ion, and 5p orbital of the I^- ion as a ligand, causing the metal–ligand charge transfer, carrier generation, and diffusion related to mobility as the photovoltaic parameter. The molecular dynamics indicate more dynamic stability and crystal formation for the Gd^{2+}-doped $FAPbI_3$ crystal rather than the $FAPbI_3$ crystal while suppressing the decomposition with the separation of the N-H band on FA. The first-principle calculation analysis predicts that it is advantageous to apply the Gd^{2+}-$FAPbI_3$-doped crystal to the perovskite solar cell, providing it with stability of photovoltaic performance.

Author Contributions: Conceptualization, A.S.; methodology, A.S.; software, A.S.; validation, A.S.; formal analysis, A.S.; investigation, A.S.; resources, A.S.; data curation, A.S.; writing—original draft preparation, A.S.; writing—review and editing, A.S. and T.O.; visualization, A.S.; supervision, T.O.; project administration, A.S. and T.O.; funding acquisition, A.S. and T.O. All authors have read and agreed to the published version of the manuscript.

Funding: This research was funded by JSPS KAKENHI Grant Number JP21K05261.

Institutional Review Board Statement: Not applicable.

Informed Consent Statement: Not applicable.

Data Availability Statement: All data generated and analyzed during this study are included in this published paper.

Conflicts of Interest: The authors declare no conflict of interest.

References

1. Li, C.; Wang, X.; Bi, E.; Jiang, F.; Park, S.M.; Li, Y.; Chen, L.; Wang, Z.; Zeng, L.; Chen, H.; et al. Rational design of Lewis base molecules for stable and efficient inverted perovskite solar cells. *Science* **2023**, *379*, 690–694. [CrossRef]
2. Li, Z.; Wang, X.; Wang, Z.; Shao, Z.; Hao, L.; Rao, Y.; Chen, C.; Liu, D.; Zhao, Q.; Sun, X.; et al. Ammonia for post-healing of formamidinium-based Perovskite films. *Nat. Commun.* **2022**, *13*, 4417. [CrossRef] [PubMed]
3. Wu, Y.; Wang, Q.; Chen, Y.; Qiu, W.; Peng, Q. Stable perovskite solar cells with 25.17% efficiency enabled by improving crystallization and passivating defects synergistically. *Energy Environ. Sci.* **2022**, *15*, 4700–4709. [CrossRef]
4. Wu, X.; Zhang, D.; Wang, X.; Jiang, X.; Liu, B.; Li, B.; Li, Z.; Gao, D.; Zhang, C.; Wang, Y.; et al. Eco-friendly perovskite solar cells: From materials design to device processing and recycling. *EcoMat* **2023**, *5*, e12352. [CrossRef]
5. Ono, I.; Oku, T.; Suzuki, A.; Asakawa, Y.; Terada, S.; Okita, M.; Fukunishi, S.; Tachikawa, T. Fabrication and characterization of $CH_3NH_3PbI_3$ solar cells with added guanidinium and inserted with decaphenylpentasilane. *Jpn. J. Appl. Phys.* **2022**, *61*, SB1024. [CrossRef]

6. Okumura, R.; Oku, T.; Suzuki, A.; Okita, M.; Fukunishi, S.; Tachikawa, T.; Hasegawa, T. Effects of adding alkali metals and organic cations to Cu-based perovskite solar cells. *Appl. Sci.* **2022**, *12*, 1710. [CrossRef]
7. Enomoto, A.; Suzuki, A.; Oku, T.; Okita, M.; Fukunishi, S.; Tachikawa, T.; Hasegawa, T. Effects of Cu, K and guanidinium addition to $CH_3NH_3PbI_3$ perovskite solar cells. *J. Electron. Mater.* **2022**, *51*, 4317–4328. [CrossRef]
8. Asakawa, Y.; Oku, T.; Kido, M.; Suzuki, A.; Okumura, R.; Okita, M.; Fukunishi, S.; Tachikawa, T.; Hasegawa, T. Fabrication and characterization of $SnCl_2$- and CuBr-added perovskite photovoltaic devices. *Technologies* **2022**, *10*, 112. [CrossRef]
9. Terada, S.; Oku, T.; Suzuki, A.; Okita, M.; Fukunishi, S.; Tachikawa, T.; Hasegawa, T. Ethylammonium bromide- and potassium-added $CH_3NH_3PbI_3$ perovskite solar cells. *Photonics* **2022**, *9*, 791. [CrossRef]
10. Enomoto, A.; Suzuki, A.; Oku, T.; Fukunishi, S.; Tachikawa, T.; Hasegawa, T. First-principles calculations and device characterizations of formamidinium-cesium lead triiodide perovskite crystals stabilized by germanium or copper. *Jpn. J. Appl. Phys.* **2023**, *62*, SK1015. [CrossRef]
11. Hossain, M.K.; Toki, G.F.I.; Kuddus, A.; Rubel, M.H.K.; Hossain, M.M.; Bencherif, H.; Rahman, M.F.; Islam, M.R.; Mushtaq, M. An extensive study on multiple ETL and HTL layers to design and simulation of high-performance lead-free $CsSnCl_3$-based perovskite solar cells. *Sci. Rep.* **2023**, *13*, 2521. [CrossRef] [PubMed]
12. Hossain, M.K.; Mohammed, M.K.A.; Pandey, R.; Arnab, A.A.; Rubel, M.H.K.; Hossain, K.M.; Ali, M.H.; Rahman, M.F.; Bencherif, H.; Madan, J.; et al. Numerical analysis in DFT and SCAPS-1D on the influence of different charge transport layers of $CsPbBr_3$ perovskite solar cells. *Energy Fuels* **2023**, *37*, 6078. [CrossRef]
13. Hossain, M.K.; Toki, G.F.I.; Samajdar, D.P.; Mushtaq, M.; Rubel, M.H.K.; Pandey, R.; Madan, J.; Mohammed, M.K.A.; Islam, M.R.; Rahman, M.F.; et al. Deep insights into the coupled optoelectronic and photovoltaic analysis of lead-free $CsSnI_3$ perovskite-based solar cell using DFT calculations and SCAPS-1D simulations. *ACS Omega* **2023**, *8*, 22466–22485. [CrossRef]
14. Diao, X.; Diao, Y.; Tang, Y.; Zhao, G.; Gu, Q.; Xie, Y.; Shi, Y.; Zhu, P.; Zhang, L. High-throughput screening of stable and efficient double inorganic halide perovskite materials by DFT. *Sci. Rep.* **2022**, *12*, 12633. [CrossRef]
15. Ma, C.; Eickemeyer, F.T.; Lee, S.H.; Kang, D.H.; Kwon, S.J.; Grätzel, M.; Park, N.G. Unveiling facet-dependent degradation and facetengineering for stable perovskite solar cells. *Science* **2023**, *379*, 173–178. [CrossRef] [PubMed]
16. Chin, X.Y.; Turkay, D.; Steele, J.A.; Tabean, S.; Eswara, S.; Mensi, M.; Fiala, P.; Wolff, C.M.; Paracchino, A.; Artuk, K.; et al. Interface passivation for 31.25%-efficient perovskite/silicon tandem solar cells. *Science* **2023**, *381*, 59–63. [CrossRef]
17. Xia, J.; Liang, C.; Gu, H.; Mei, S.; Li, S.; Zhang, N.; Chen, S.; Cai, Y.; Xing, G. Surface passivation toward efficient and stable perovskite solar cells. *Energy Environ. Mater.* **2023**, *6*, e12296. [CrossRef]
18. Ren, J.; Liu, T.; He, B.; Wu, G.; Gu, H.; Wang, B.; Li, J.; Mao, Y.; Chen, S.; Xing, G. Passivating defects at the bottom interface of perovskite by ethylammonium to improve the performance of perovskite solar cells. *Small* **2022**, *18*, 2203536. [CrossRef] [PubMed]
19. Azmi, R.; Ugur, E.; Seitkhan, A.; Aljamaan, F.; Subbiah, A.S.; Liu, J.; Harrison, G.T.; Nugraha, M.I.; Eswaran, M.K.; Babics, M.; et al. Damp heat–stable perovskite solar cells with tailored-dimensionality 2D/3D heterojunctions. *Science* **2022**, *376*, 73–77. [CrossRef]
20. Fu, Y.; Li, Y.; Xing, G.; Cao, D. Surface passivation of perovskite with organic hole transport materials for highly efficient and stable perovskite solar cells. *Mater. Mater. Today Adv.* **2022**, *16*, 100300. [CrossRef]
21. Lin, R.; Xu, J.; Wei, M.; Wang, Y.; Qin, Z.; Liu, Z.; Wu, J.; Xiao, K.; Chen, B.; Park, S.M.; et al. All-perovskite tandem solar cells with improved grain surface passivation. *Nature* **2022**, *603*, 73–78. [CrossRef]
22. Suzuki, A.; Hasegawa, R.; Funayama, K.; Oku, T.; Okita, M.; Fukunishi, S.; Tachikawa, T.; Hasegawa, T. Additive effects of $CuPcX_4$-TCNQ on $CH_3NH_3PbI_3$ perovskite solar cells. *J. Mater. Sci. Mater. Electron.* **2023**, *34*, 588. [CrossRef]
23. Ogawa, C.; Suzuki, A.; Oku, T.; Fukunishi, S.; Tachikawa, T.; Hasegawa, T. Metallophtalocyanine used interface engineering for improving long-term stability of methylammonium lead triiodide perovskite. *Phys. Status Solidi A* **2023**, *220*, 2300038. [CrossRef]
24. Kachhap, S.; Singh, S.; Singh, A.K.; Singh, S.K. Lanthanide-doped inorganic halide perovskites ($CsPbX_3$): Novel properties and emerging applications. *J. Mater. Chem. C* **2022**, *10*, 3647. [CrossRef]
25. Samanta, T.; Mukurala, N.; Viswanath, N.S.M.; Han, J.H.; Cho, H.B.; Min, J.W.; Jung, S.W.; Park, Y.; Chung, W.J.; Im, W.B. Recent progress in lanthanide-based metal halide perovskites: Synthesis, properties, and applications. *Opt. Mater. X* **2023**, *18*, 100238. [CrossRef]
26. Wang, L.; Zhou, H.; Hu, J.; Huang, B.; Sun, M.; Dong, B.; Zheng, G.; Huang, Y.; Chen, Y.; Li, L.; et al. A Eu^{3+}-Eu^{2+} ion redox shuttle imparts operational durability to Pb-I perovskite solar cells. *Science* **2019**, *363*, 265–270. [CrossRef] [PubMed]
27. Mir, W.J.; Sheikh, T.; Arfin, H.; Xia, Z.; Nag, A. Lanthanide doping in metal halide perovskite nanocrystals: Spectral shifting, quantum cutting and optoelectronic applications. *NPG Asia Mater.* **2020**, *12*, 9. [CrossRef]
28. Lee, M.; Lee, D.H.D.; Hong, S.V.; Woo, H.Y.; Chae, J.-Y.; Lee, D.W.; Han, M.J.; Paik, T. Highly luminescent and multifunctional zero-dimensional cesium lanthanide chloride (Cs_3LnCl_6) colloidal nanocrystals. *Adv. Opt. Mater.* **2022**, *10*, 2102727. [CrossRef]
29. Zhang, L.; Yuan, M. Lanthanide doped lead-free double perovskites as the promising next generation ultra-broadband light sources. *Light Sci. Appl.* **2022**, *11*, 99. [CrossRef]
30. Yang, Y.; Wu, J.; Wang, X.; Guo, Q.; Liu, X.; Sun, W.; Wei, Y.; Huang, Y.; Lan, Z.; Huang, M.; et al. Suppressing vacancy defects and grain boundaries via ostwald ripening for high-performance and stable perovskite solar cells. *Adv. Mater.* **2020**, *32*, 1904347. [CrossRef]
31. Suzuki, A.; Kishimoto, K.; Oku, T.; Okita, M.; Fukunishi, S.; Tachikawa, T. Additive effect of lanthanide compounds into perovskite layer on photovoltaic properties and electronic structures. *Synth. Met.* **2022**, *287*, 117092. [CrossRef]

32. Suzuki, A.; Oku, T. Electronic structures and molecular dynamics of gadolinium-doped $FAPbI_3$ perovskite crystals. *Jpn. J. Appl. Phys.* **2023**, *62*, SK1006. [CrossRef]
33. Fransson, E.; Rosander, P.; Eriksson, F.; Rahm, J.M.; Tadano, T.; Erhart, P. Limits of the phonon quasi-particle picture at the cubic-to-tetragonal phase transition in halide perovskites. *Commun. Phys.* **2023**, *6*, 173. [CrossRef]
34. Kaiser, W.; Mosconi, E.; Alothman, A.A.; Meggiolaro, D.; Gagliardi, A.; Angelis, F.D. Halide-driven formation of lead halide perovskites: Insight from ab initio molecular dynamics simulations. *Mater. Adv.* **2021**, *2*, 3915–3926. [CrossRef]
35. Ning, J.; Zheng, L.; Lei, W.; Wang, S.; Xi, J.; Yang, J. Temperature-dependence of the band gap in the all-inorganic perovskite $CsPbI_3$ from room to high temperatures. *Phys. Chem. Chem. Phys.* **2022**, *24*, 16003–16010. [CrossRef]
36. Kaiser, W.; Ricciarelli, D.; Mosconi, E.; Alothman, A.A.; Ambrosio, F.; Angelis, F.D. Stability of tin-versus lead-halide perovskites: Ab initio molecular dynamics simulations of perovskite/water interfaces. *J. Phys. Chem. Lett.* **2022**, *13*, 2321–2329. [CrossRef] [PubMed]
37. Tseng, M.-L.; Adesiyan, A.; Gassoumi, A.; Gorji, N.E. A molecular dynamics study of water confined in between two graphene sheets under compression. *J. Nanopart. Res.* **2023**, *25*, 51. [CrossRef]
38. Arora, N.; Greco, A.; Meloni, S.; Hinderhofer, A.; Mattoni, A.; Rothlisberger, U.; Hagenlocher, J.; Caddeo, C.; Zakeeruddin, S.M.; Schreiber, F.; et al. Kinetics and energetics of metal halide perovskite conversion reactions at the nanoscale. *Commun. Mater.* **2022**, *3*, 22. [CrossRef]
39. Shi, R.; Guo, M.; Long, R. Improved defect tolerance and charge carrier lifetime in tin–lead mixed perovskites: Ab Initio quantum dynamics, *J. Phys. Chem. Lett.* **2023**, *14*, 499–507. [CrossRef]
40. Weller, M.T.; Weber, O.J.; Frost, J.M.; Walsh, A. Cubic perovskite structure of black formamidinium lead iodide, α-$[HC(NH_2)_2]PbI_3$, at 298 K. *J. Phys. Chem. Lett.* **2015**, *6*, 3209–3212. [CrossRef]
41. Mashiyama, H.; Kurihara, Y.; Azetsu, T. Disordered cubic perovskite structure of $CH_3NH_3PbX_3$ (X = Cl, Br, I). *J. Korean Phys. Soc.* **1998**, *32*, S156–S158.
42. Oku, T. Crystal structures of perovskite halide compounds used for solar cells. *Rev. Adv. Mater. Sci.* **2020**, *59*, 264–305. [CrossRef]